



# On the Influence of Temperature and Number of Passes on the Mechanical Properties of an Al–Mg Alloy Processed by Cyclic Expansion Extrusion

V. Babu<sup>1</sup> · Balasivanandha Prabu Shanmugavel<sup>1</sup> · K. A. Padmanabhan<sup>1</sup>

Received: 10 March 2020 / Accepted: 1 June 2020 / Published online: 19 June 2020  
© The Korean Institute of Metals and Materials 2020

## Abstract

The influence of working temperature and number of passes on the mechanical properties of aluminium alloy, AA 5083, processed by cyclic expansion and extrusion (CEE) is discussed. The specimens were processed up-to 10 CEE passes at 200 °C, 300 °C and 400 °C. The average grain size of the starting annealed material was  $84.5 \pm 6.8 \mu\text{m}$ , with 39.4% being of the high-angle grain boundaries (HAGBs) type. After 8 CEE passes at 200 °C the material had an average grain size of  $3.3 \pm 0.6 \mu\text{m}$  and 41.3% of the grain boundaries were of the high-angle type (HAGBs). The combined effect of an increase in dislocation density and reduction in grain size as a result of CEE processing contributed to an increase in hardness and strength of the alloy. At 200 °C, the specimen exhibited uniform hardness values with a maximum improvement of 104% after 8 passes and the ultimate tensile strength had also increased by 64% compared with the unprocessed condition. However, the mechanical properties decreased in the specimens that were processed at the higher temperatures of 300 °C and 400 °C.

**Keywords** Al–Mg alloy · Cyclic expansion extrusion · Grain refinement · Microstructure

## 1 Introduction

Due to their high strength and light weight, Al–Mg alloys are used as structural materials in automotive and aerospace applications. In recent years, attention is focused on improving the metallurgical/mechanical and physical properties of these alloys [1]. Production of ultrafine grained materials through severe plastic deformation (SPD) techniques has been a well-established route [2–4]. These techniques have the ability to produce materials with good mechanical properties, namely, high hardness, high tensile strength, improved fatigue life and enhanced ductility (at least in some cases) at low temperatures [2]. Several SPD methods, namely, equal channel angular pressing (ECAP) [5], accumulative roll bonding (ARB) [6], cyclic extrusion compression (CEC) [7], repetitive corrugation and straightening (RCS) [8], repetitive upsetting extrusion (RUE) [9], multi-directional forging

(MDF) [10], multi-channel spiral twist extrusion (MCSTE) [11] and cyclic expansion extrusion (CEE) [12] have been used to produce ultrafine grain-(UFG)/nano-structures-(NS) in non-ferrous metals and alloys.

Among the different SPD techniques developed, ECAP, CEC and CEE are very popular for developing UFG structure in rod/bar like material [11]. In contrast, ARB and RCS techniques are used to develop UFG microstructures in sheet materials. The use of accumulative roll bonding process is limited due to lack of bonding at the interfaces of different layers [13]. However, the recent work of Ebrahimi et al. [6] established that fine distributions of the secondary phase and extraordinary reduction in grain size are obtainable in the aluminum alloy Al–Zn–Mg–Cu processed by the ARB technique. The tensile strength and the microhardness values were increased with increasing number of cycles of ARB [6]. The RCS process suffers due to inhomogeneous strain application resulting in inhomogeneous microstructure formation [14]. This problem can be eliminated by a proper selection of die geometry [8], working temperature and strain path [15, 16].

Cyclic expansion extrusion (CEE) is one of the recently developed SPD techniques [12]. The equipment and tooling are simple and are suited to develop UFG structures in

✉ V. Babu  
vbabume@gmail.com

<sup>1</sup> Department of Mechanical Engineering, College of Engineering Guindy, Anna University, Chennai 600025, India

bulk materials without much change in the initial dimensions of the specimen. Hansen [17] reported that dislocation multiplication, grain boundary strengthening and formation of fine grains are responsible for the improvements in mechanical properties. Extensive studies were conducted on different aluminium alloys to identify the effect of working temperature on microstructure formation and the resultant mechanical properties [18–20]. Mazurina et al. [21] reported the role of temperature (in the range of 250–475 °C) on aluminium 2219 alloy processed by ECAP. An increase in the pressing temperature (temperatures 400 °C and 475 °C) led to a decrease in the volume fraction of new grains and an increase in the average grain size. This could be attributed to the relaxation of strain incompatibilities at grain boundaries due to dynamic recovery and sliding. At processing temperatures of 250 °C and 300 °C, new UFGs with a size in a sub-micron range were fully developed almost in an entire area. In contrast, colonies of strain-induced UFGs with HAGBs were mixed with coarse grains containing sub-grains with LAGBs at the higher processing temperatures of 400 °C and 475 °C [21].

Goloborodko et al. [22] studied the microstructure of Al 7475 alloy after ECAP, carried out at elevated temperatures in the range of 250–400 °C. The average grain size increases with an increase in temperature and the grain size becomes more homogeneous and transverse crystallite size is approximately constant with increasing temperature. Increase in temperature tends to delay the transformation rate from low-angle grain boundaries (LAGBs) to high-angle grain boundaries (HAGBs) at medium strain ranges. New grains with HAGBs were developed only at higher strain ranges at lower processing temperatures due to a high density of precipitation leading to low recovery rate [22].

Previous studies by the present authors revealed that in aluminium alloy AA 6063 subjected to CEE up-to 10 passes at 200 °C [semi-die angle ( $\alpha$ ) of 22.5° at a ram velocity of 1 mm/s], the average grain size had decreased from 20  $\mu\text{m}$  in the parent material to  $\sim 4.8 \mu\text{m}$  after 4 passes. At the end of 10 passes there was a slight increase in the average grain size, with 40% of the grain boundaries being of the HAGB type. The hardness and strength values increased as a result of CEE. However, elongation to failure decreased with increasing number of passes. The specimen after 4 passes had a hardness value improvement of about 40% and a tensile strength increase of 23% compared with that of the unprocessed (annealed) alloy [23]. It is also worthy of note that in SPD processes, high temperatures favor specimen deformation without cracks/fracture [18, 24].

In the present work the Al–Mg alloy (AA 5083), was investigated. For understanding the mechanism of grain refinement, microstructure and mechanical properties of AA 5083, specimens processed using CEE dies [semi-die angle ( $\alpha$ ) of 30°] at three different temperatures (200 °C, 300 °C and 400 °C)

were examined after every 2 passes. AA 5083 was a non-age hardenable alloy, which demonstrates interesting properties as a structural material, including high strength and excellent corrosion resistance. These merits of AA 5083 are attractive in special applications, such as vehicles body sheet metal [25, 26].

In AA 5083 alloy, the precipitate particles ( $\text{Mg}_2\text{Al}_3$ ) are an intermetallic compound [27, 28]. The influence of SPD on this Al–Mg alloy is interesting. At elevated temperatures the flow stress is very much enhanced, i.e., around three times but the ductility decreases [29]. These changes are attributed to the influence of the  $\text{Mg}_2\text{Al}_3$  particles in reducing the dislocations mobility and recovery rate in the aluminium alloys. However, it is also important to understand the effects of alloying elements on the formation of solid solution and refinement of grains in attaining an UFG structure [30]. Microstructure homogeneity could be achieved by imposing strain control, e.g. optimizing die profile, pressing velocity, and temperature [8]. Influence of temperature on grain refinement during the CEE process is not discussed properly in literature. Influence of temperature on grain refinement in different alloys has been examined using ECAP and RCS processes [15, 21, 22]. Solid solution strengthening arises in 5xxx alloys due to the addition of magnesium. Aluminium could hold more magnesium than silicon and manganese in solid solution. As a result, better solid solution strengthening is possible in 5xxx alloys than in 6xxx alloys. Moreover, in the 5xxx alloy the formation of Al–Mg particles results in higher strength than in 6xxx alloy. These particles act as obstacles to dislocation motion.

Based on literature survey concerning SPD processing, it was clearly understood that the effect of temperature and the number of passes in obtaining a homogenous UFG structure in materials is significant [15, 19, 22, 31, 32]. The literature [15, 21, 31, 33] further suggests that the specimens processed at higher temperatures exhibit inferior mechanical properties due to inefficient grain refinement. However, elevated temperature deformation leads to homogeneous microstructures. In those studies, the effect of temperature on the CEE process has been left unexplored. Therefore, in this present investigation the Al–Mg alloy, AA 5083, was processed at different temperatures in the range 200–400 °C with multiple passes of CEE. In addition to the effect of processing temperature, the effect of the number of passes on microstructure evolution and mechanical properties were also examined. Furthermore, the present work considers grain refinement homogeneity as a function of the experimental conditions.

## 2 Experimental Process

Commercial Al–Mg alloy, AA 5083, containing (wt%): Al-96.63, Mg-2.08, Mn-0.3, Fe-0.35, Si-0.39%, Cr-0.16%, Cu-0.07% Zn-0.005 and Ti-0.015% was used in this study.

The as-received alloy was machined to specimens of 18 mm diameter and 127 mm length. The specimens were then annealed at 580 °C for 3 h. The CEE die has a semi-die angle ( $\alpha$ ) of 30°. The CEE process was carried out in a 50kN hydraulic press with a ram velocity of 2.5 mm/s (equivalent to a strain rate of  $1.97 \times 10^{-2} \text{ s}^{-1}$  for the present dimensions of the specimen). In order to reduce the friction between the die wall and the specimen, graphite paste was used as a lubricant. The specimen and die were heated in a closed muffle-type furnace. The entire CEE processing was done under isothermal condition. The processing temperature was maintained using a temperature controller and the temperature was measured using a thermocouple located inside the muffle furnace.

Figure 1 shows schematic representation of the CEE process. An expansion and an extrusion step together was considered as a single CEE pass [23]. The die was turned 180° up-side down after every pass. The unprocessed and CEE processed specimens were cut according to the ASTM-E8M standard for the tensile tests, which were tested using an INSTRON testing machine at a velocity of 0.05 mm/s. The hardness test was carried out using a Vickers microhardness machine (Wilson Wolpert, Germany) with a load of 0.5 kg and a dwell time of 15 s. Before and after CEE processing, ten hardness readings were taken on the specimens along the extrusion direction at uniform intervals and

averaged. Three specimens were prepared from the processed samples along the extrusion direction. For getting consistent readings, three specimens were tested for every case. Orientation image microscopy (OIM) and TEM were employed to understand the grain refinement mechanism. The OIM maps indicate the orientations of the grains represented in the images. The grains size and misorientations were calculated using the integrated arrangement attached to the OIM system taking into account the scanned area and the densities of grain boundaries (i.e., low- and high-angle boundary area fractions) [14]. Misorientation less than 15° (misorientation between 1.5° and 15°) is considered as low-angle grain boundaries (LAGBs), while high-angle grain boundaries (HAGBs) display misorientations more than 15° ( $> 15^\circ$ ) [34]. The specimens for microscopy and TEM analysis were prepared by the usual metallographic procedures of electro-polishing.

## 3 Results

### 3.1 Hardness

Figure 2 shows the results of hardness, for specimens processed at different temperatures, viz. 400 °C, 300 °C and 200 °C up-to 10 passes. It is noticed that the specimen

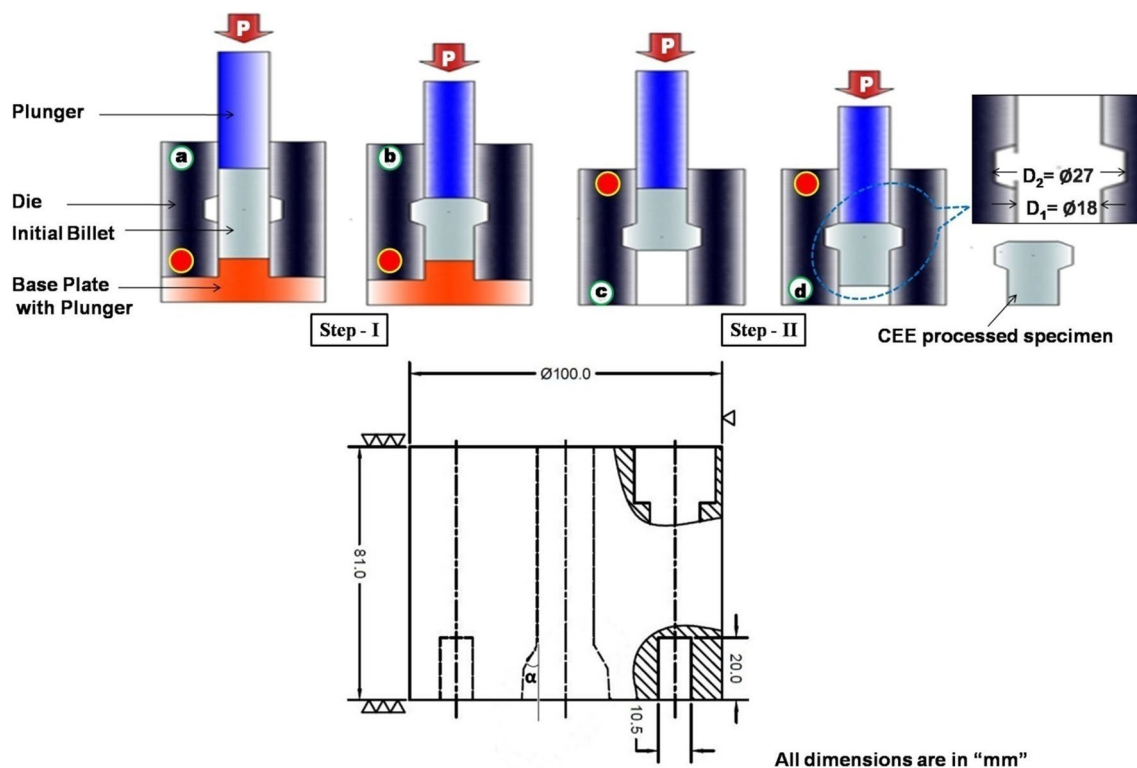


Fig. 1 A schematic representation of CEE process with die profile

processed at 400 °C showed only a marginal increase in hardness up-to 10 passes (Fig. 2a). The unprocessed alloy (annealed condition) displayed an average hardness value of  $51 \pm 1.9\text{HV}$ . The average hardness of the Al–Mg alloy had increased to  $65 \pm 1.2\text{HV}$  after 2 passes at 400 °C. There were no significant changes in hardness after 4 and 8 passes. A hardness value of  $82 \pm 1.2\text{HV}$  was reached at the end of 10 passes—see Fig. 2a.

Figure 2b, c display the micro-hardness values of the specimens processed at 300 °C and 200 °C respectively, which proves that a lower processing temperature leads to a higher hardness value. Figure 2b shows the hardness of the specimen processed at 300 °C. It is evident that the micro-hardness of the alloy increased to  $87 \pm 3.1\text{HV}$  after two passes, which is a slightly higher value (9%) compared with the value obtained for a specimen processed at 400 °C by the same number of passes. The hardness values ( $89 \pm 1.4\text{HV}$ ) do not show any significant changes up-to 6 passes. However, due to annihilation of dislocations and dynamic recrystallization (DRX) the hardness values decreased to  $84 \pm 2.8\text{HV}$  and  $81 \pm 3.3\text{HV}$  respectively after 8 and 10 passes at 300 °C.

The hardness values of a specimen processed at 200 °C showed a good increase after every pass (Fig. 2c). After 8 passes, the hardness reached a value of  $104 \pm 0.6\text{HV}$ . However, the hardness value decreases to  $96 \pm 2.6\text{HV}$  at the end of 10 passes due to dynamic re-crystallization. But, this value is clearly greater than what is found at 400 °C and 300 °C. Figure 2d displays the hardness values after every

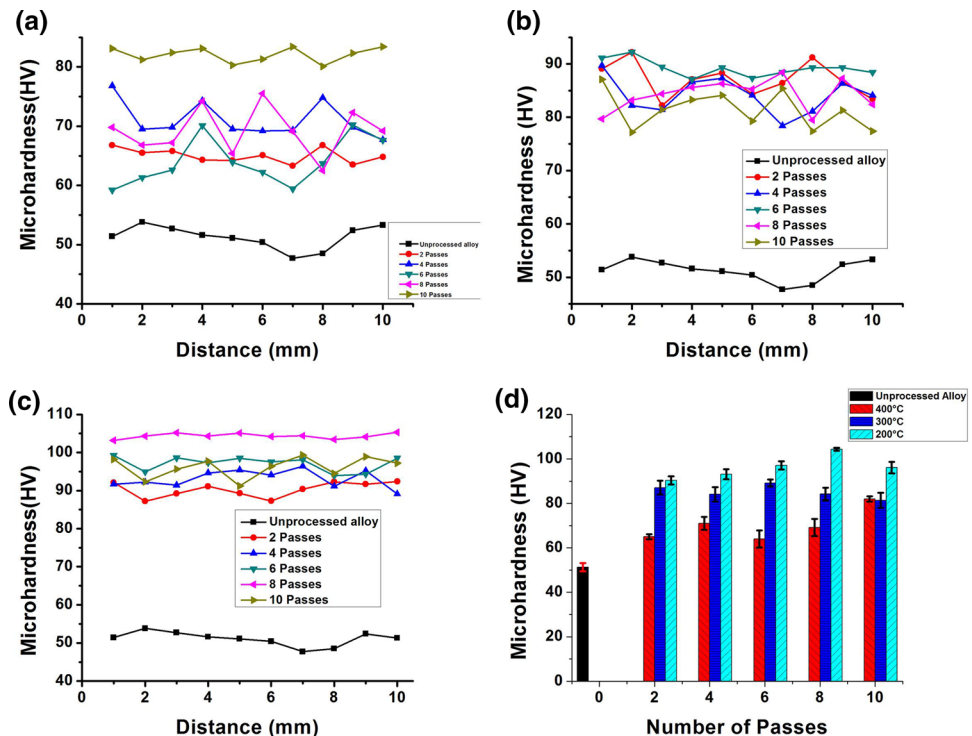
pass at different temperatures. It is worthy of note that at the higher temperatures improvement in hardness was not significant. At 200 °C, the micro-hardness values in different locations of the specimen at the end of 8 passes have a homogeneous distribution and are also higher, which could be attributed to significant grain refinement [5, 35].

### 3.2 Tensile Behavior

Figure 3 shows the stress–strain curves of the unprocessed and CEE processed specimens. CEE processing increased the strength of the alloy, but the magnitude of increase depended on the processing temperature. The increase in strength is marginal at a processing temperature of 400 °C—Fig. 3a. At this temperature the strength increased up-to 4 CEE passes. Compared to the unprocessed material, after 4 passes the YS increased to  $116 \pm 2\text{ MPa}$  from the parent material value of  $93 \pm 4.2\text{ MPa}$  and UTS had increased to  $138 \pm 2.8\text{ MPa}$  from the parent material value of  $124.5 \pm 9.2\text{ MPa}$ . The elongation at fracture had increased to  $26.1 \pm 1.4\%$  from the parent material value of  $24.9 \pm 0.7\%$ . The YS and UTS values did not increase much beyond this stage as it only reached  $121 \pm 1\text{ MPa}$  and  $140 \pm 0.7\text{ MPa}$  respectively even at the end of 10 passes. However, there was an increase in the elongation to failure from  $24.9 \pm 0.7$  to  $36.1 \pm 0.5\%$  compared with the unprocessed alloy at 400 °C, as shown in Fig. 3a.

At 300 °C (Fig. 3b) the YS and UTS were  $124 \pm 1$  and  $148 \pm 0.7\text{ MPa}$  respectively at the end of two passes, which

**Fig. 2** Hardness values of alloy Al 5083 at three different temperatures: **a** processed at 400 °C, **b** processed at 300 °C, **c** processed at 200 °C, compared with the hardness of the unprocessed alloy, and **d** a histogram presents a comparison of the average hardness values of the processed material at the three temperatures with that of the unprocessed alloy





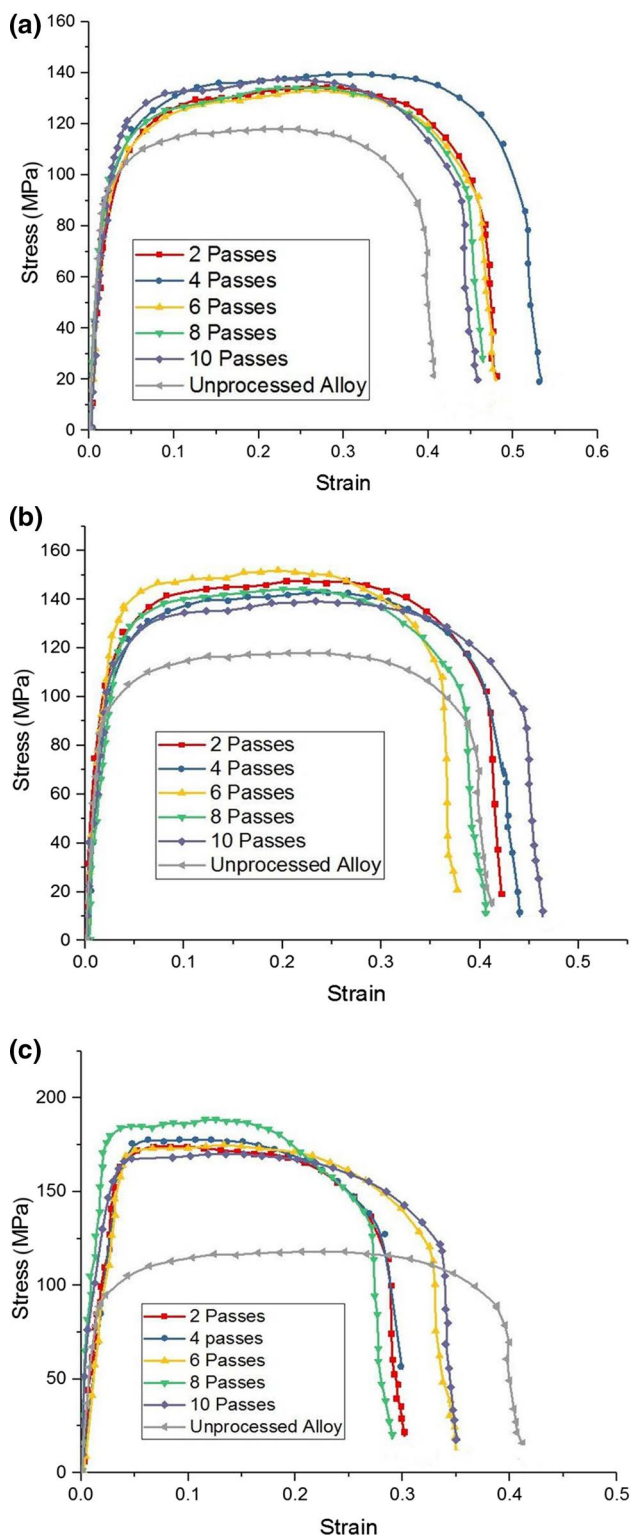


**Fig. 3** Stress—strain curves for alloy AA 5083 **a** processed at 400 °C, **b** processed at 300 °C and **c** processed at 200 °C. Stress—strain curve of the same alloy in an unprocessed condition is also given for comparison

decreased to  $121 \pm 0.9$  and  $143 \pm 1.4$  MPa after 4 passes to reach  $131 \pm 1.6$  and  $152 \pm 0.7$  MPa after 6 passes of CEE respectively. In contrast, the elongation to fracture had increased to  $26.4 \pm 0.3\%$  after 2 passes, to  $26.6 \pm 0.2\%$  at the end of 4 passes and decreased to  $22.8 \pm 0.9\%$  after 6 passes. After 8 and 10 passes, the YS and UTS values decreased to  $123 \pm 0.9$ ,  $145 \pm 0.7$  MPa and  $121 \pm 2$ ,  $140 \pm 2.8$  MPa respectively, while the corresponding elongations to fracture were  $22.5 \pm 1.2\%$  and  $25.1 \pm 1.2\%$  respectively. Thus the changes in the UTS and elongation to fracture values did not parallel each other and repetitions of the experiments are needed to check if the values reported here are reproducible.

At 200 °C (Fig. 3c) up-to 6 passes, the YS and UTS values hardly changed; the values of YS after 2, 4 and 6 passes were  $152 \pm 4$  MPa,  $158 \pm 3$  MPa and  $152 \pm 2$  MPa respectively and the UTS values were  $175 \pm 7.7$  MPa,  $178 \pm 2.1$  MPa and  $174 \pm 1.4$  MPa respectively. Likewise, the elongation to fracture also oscillated within a narrow range:  $15.4 \pm 1.6\%$ ,  $14.1 \pm 0.3\%$  and  $16.4 \pm 0.8\%$  after 2, 4 and 6 passes respectively. After 8 passes, the YS value reached  $167 \pm 2$  MPa and the maximum UTS for the campaign at this temperature of  $189 \pm 2.1$  MPa was reached, but the elongation to fracture fell to  $15.6 \pm 0.3\%$ . After 10 passes the YS and UTS decreased to  $148 \pm 0.3$  and  $170 \pm 0.7$  MPa respectively, while the elongation to fracture increased to  $19.5 \pm 3.4\%$ , both indicative of dynamic re-crystallization. It is interesting that up-to the end of 8 passes, even though the UTS had clearly increased, the loss in elongation to fracture was not significant. Evidently, in the present set of experiments, the strength increase was maximum at 200 °C, but there was a corresponding loss in elongation to fracture compared with the other temperatures. Further, Fig. 3c reveals that the UTS value increased up-to 8 passes at 200 °C. After 10 passes, however, there was a slight decrease in the UTS value.

Table 1 shows that the YS, UTS and percentage of elongation (EL) values for the AA 5083 alloy subjected to CEE at 400 °C, 300 °C and 200 °C as well as the properties of the same alloy in an unprocessed condition. It is evident that a decrease in the processing temperature and an increase in the number of passes improve the tensile strength, but decrease the ductility.

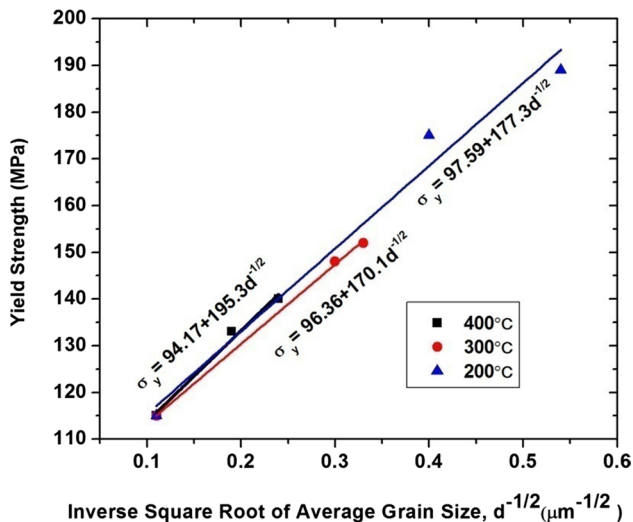
However, there was a continuous decrease in the elongation to failure up-to ten passes due to strain hardening and grain refinement. Figure 4 presents the yield stress ( $\sigma_y$ ) values against the inverse square root of the average grain size ( $d^{-1/2}$ ), which validates the Hall–Petch relationship for the different processing conditions as well as in the unprocessed alloy, viz.

$$\sigma_y = \sigma_0 + k_y d^{-1/2}$$

where  $\sigma_0$ —is the lattice friction stress and  $k_y$ —is a positive constant of yield related to the stress needed for extending

**Table 1** Comparison of tensile properties of alloy AA 5083 at different working temperatures and number of passes

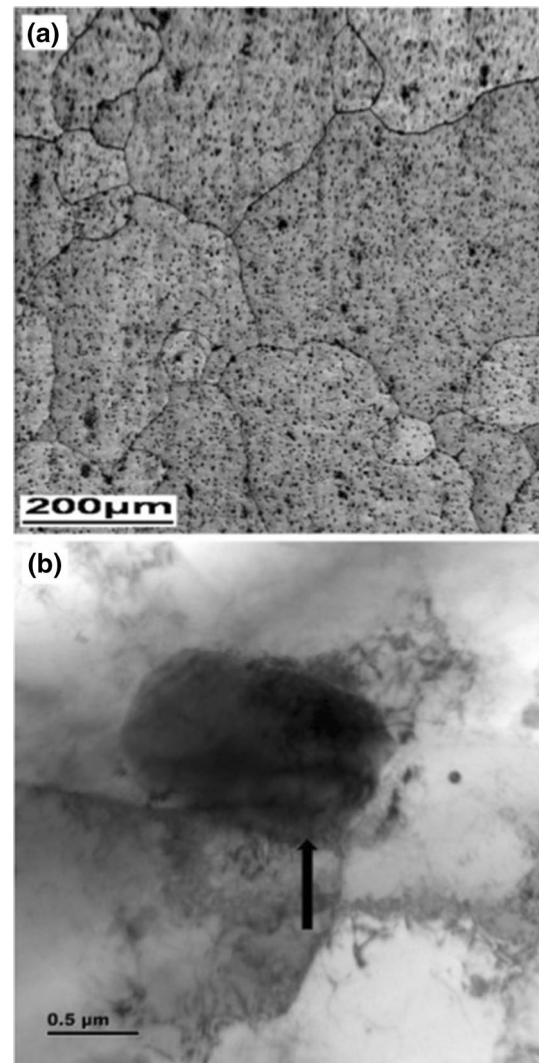
Number of passes	400 °C			300 °C			200 °C		
	YS (MPa)	UTS (MPa)	EL (%)	YS (MPa)	UTS (MPa)	EL (%)	YS (MPa)	UTS (MPa)	EL (%)
Unprocessed alloy	93	128	24.9	93	128	24.9	93	128	24.9
2nd pass	113	133	28.8	124	148	26.4	152	175	15.4
4th pass	116	138	26.1	121	143	26.6	158	178	14.1
6th pass	112	133	29.8	131	152	22.8	152	174	16.4
8th pass	115	135	25.6	123	145	22.5	167	189	15.6
10th pass	121	140	36.1	121	141	25.1	148	170	19.5

**Fig. 4** Yield stress values as a function of inverse square root of average grain size, which validates the Hall–Petch relation

the activities relating to dislocations into the adjacent unyielded grains [36].

### 3.3 Microstructure Analysis

Figure 5a is the OIM image of an unprocessed (annealed) specimen. It shows a coarse grained structure with an average grain size of  $84.5 \pm 6.8 \mu\text{m}$ , as measured using the linear intercept method. The microstructure contains predominantly low-angle grain boundaries which occupied 60.3%. Figure 5b shows a TEM micrograph of the unprocessed (annealed) specimen. A large rod-like dispersoids/precipitate (black arrow) was found in the unprocessed (annealed) alloy. The rod-like structures were identified as  $\text{Mg}_2\text{Al}_3$  precipitates or dispersoids [15, 37]. The boundaries of the coarse grains were very clear, sharp and free from dislocations. The size of the second phase precipitates was about  $1.5 \mu\text{m}$ . The microstructures of the alloy after two passes of CEE at 400 °C, 300 °C and 200 °C respectively are shown in Figs. 6a, 7a and 8a. It shows the deformation of grains, where a large shear band could be also seen in

**Fig. 5** a OIM map and b TEM micrograph of unprocessed (annealed) specimen

the micrograph due to localized plastic flow between large columnar grains [38]. The presence of shear bands is indicative of a filamentary microstructure [7]. Similar observations have also been reported by other researchers [6, 38].



The average grain size after 2 passes was  $27.3 \pm 4.6 \mu\text{m}$ ,  $11.1 \pm 2.3 \mu\text{m}$  and  $6.4 \pm 1 \mu\text{m}$  at 400 °C, 300 °C and 200 °C respectively. The elongated grains developed up-to the end of 2 passes were mostly of low-angle grain boundaries (LAGBs) type. The microstructures contained 94.2%, 85.2%, and 78.6% of LAGBs observed at processing temperatures of 400 °C, 300 °C and 200 °C respectively after 2 passes.

The microstructure of the alloy after 10 passes at 400 °C is presented in Fig. 6b, as non-equiaxed and elongated grains. The average grain size was  $17.6 \pm 2.8 \mu\text{m}$  with a LAGBs fraction of 86.3%. In contrast, the microstructure of the alloy after 6 passes at 300 °C (Fig. 7b), shows equiaxed as well as elongated grains in the extrusion direction with the average grain size of  $9.3 \pm 1.4 \mu\text{m}$ . The microstructure, once again, contained a high fraction of LAGBs (91.6%). There was a decrease in the finer grain size ( $< 1 \mu\text{m}$ ) proportion to

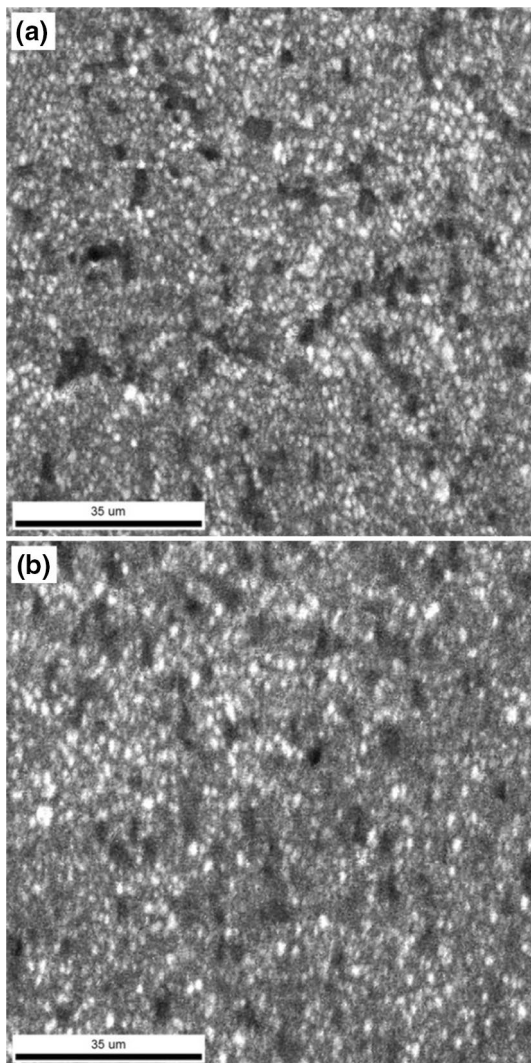


**Fig. 6** OIM maps of CEE processed Al–Mg alloy specimens at 400 °C; **a** after 2 passes, **b** after 10 passes

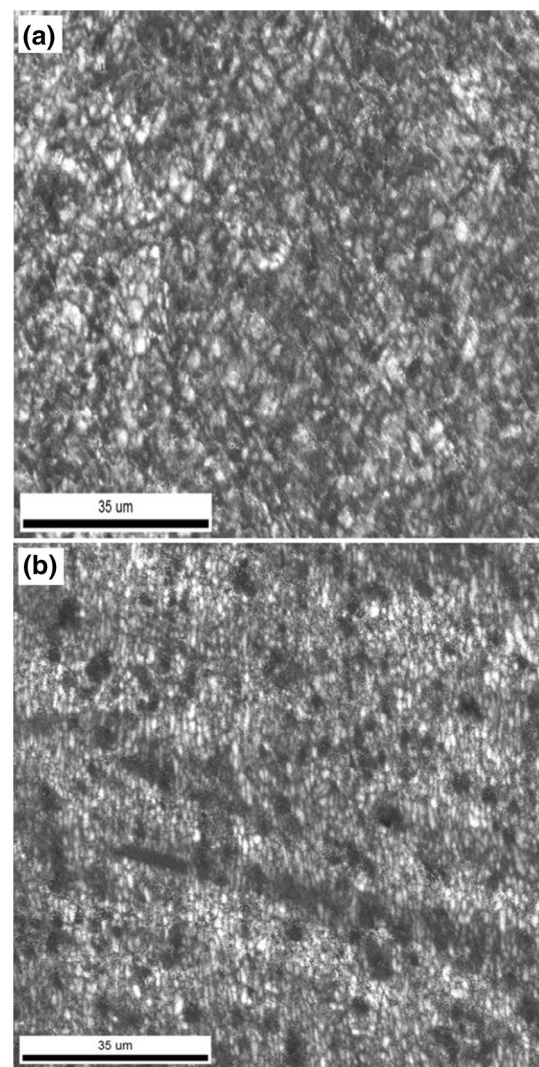


**Fig. 7** OIM maps of CEE processed Al–Mg alloy specimens at 300 °C; **a** after 2 passes, **b** after 6 passes

1.47% (6 passes at 300 °C). Many reports suggest that the alloys processed at elevated temperatures show a strength increase at relatively low strains, mainly due to increasing dislocation density and formation of sub-grains (i.e., after the initial passes). With increasing number of passes incremental strength increase becomes smaller and the dislocation densities remain almost constant [39, 40]. After 8 passes at 200 °C, the elongated grain structure is changed to an equiaxed grain structure, with fine grains. The UFG proportion has increased to 9.34% ( $< 1 \mu\text{m}$ ), with low-angle grain boundaries (LAGBs) also decreasing 58.7% (Fig. 8b). Finally, the grain refinement was homogeneous and the average grain size was  $3.3 \pm 0.6 \mu\text{m}$  after 8 passes at 200 °C. Table 2 presents the grain size distribution and fractions of misorientation angles of unprocessed and CEE processed specimens at three different temperatures.

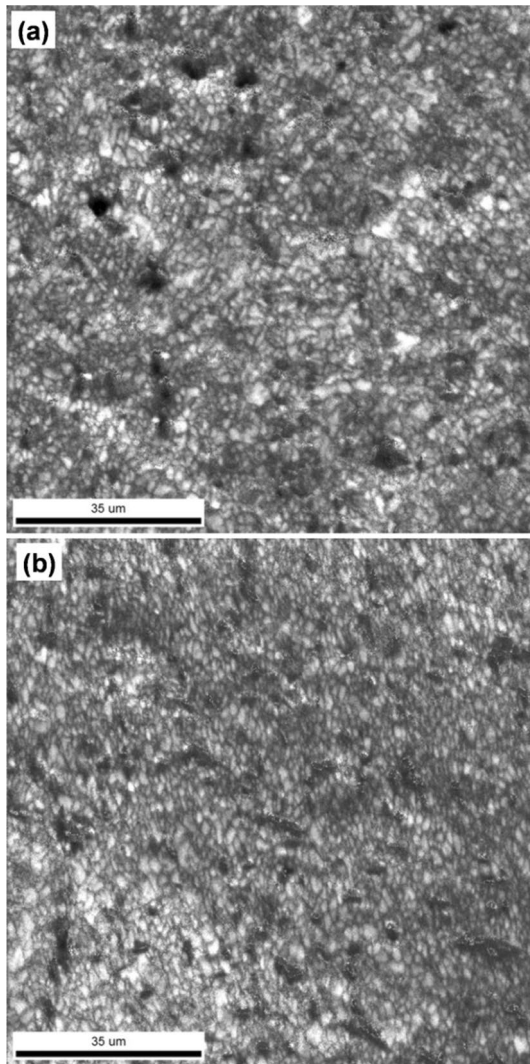


**Fig. 8** OIM maps of CEE processed Al–Mg alloy specimens at 200 °C **a** after 2 passes, **b** after 8 passes

### 3.4 TEM Analysis

High-resolution TEM images were taken to understand the formations of the ultrafine/nano-grains and precipitates in the microstructure [15, 41]. Figure 9a, b show the TEM images the specimen processed at 400 °C after 2 and 10 passes respectively. TEM micrograph of CEE processed Al–Mg alloy after 2 passes at 400 °C showed the presence of very few of dislocations with a minimum change in grain size, as shown in Fig. 9a. After 10 passes at 400 °C, ring-like and contour kinds of structures are seen in Fig. 9b. The spreading of contour (marked by a red box) is due to the movement of dislocations towards the grain boundary. The microstructure also shows evidence for sub-grain formation. Lamellar kind of deformed structures containing very few dislocations could also be observed (Fig. 9b) [3, 15].

Also, it is noted that the  $Mg_2Al_3$  precipitates size decreased to ~600 nm as a result of CEE which helps in the effective accumulation of dislocations in the vicinity of the  $Mg_2Al_3$  precipitates. But the number of second-phase precipitates (marked as red arrows) is rather small [15, 21].

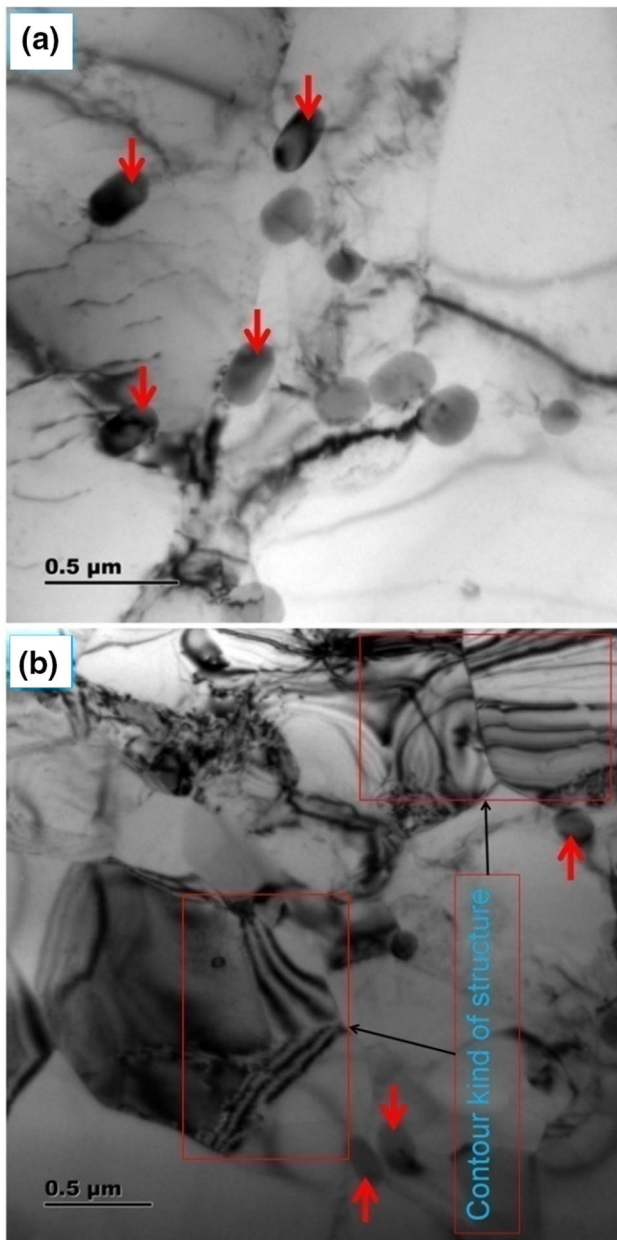
The specimen after 2 passes at 300 °C shows a similar result. However, a marginal reduction in grain size could be seen in Fig. 10a. The structure contains some fine grains (Fig. 10a). A large number of lamellar grains were formed after 6 passes (Fig. 10b). The sizes of the second phase precipitates (red arrows) were <200 nm. The thick lamellar grains are evidence of a non-homogeneous grain structure. The grain size is reduced due to dynamic re-crystallization.

Figure 11a, b correspond to TEM images after 2 and 8 passes at 200 °C. The reduction in grain size is significant. The distortion of the second-phase precipitates during plastic deformation and accumulation dislocations in the specimen after 2 passes at 200 °C are seen in Fig. 11a. The CEE process led to a relatively higher equiaxed grain refinement at 200 °C. The microstructure of the alloy after 8 passes could be observed as uniform grain refinement with a fine grain size, as shown in Fig. 11b.

**Table 2** Grain size distributions and misorientation angle details of unprocessed and CEE processed AA 5083 alloy

T (°C)	No. of passes	Avg. grain size (μm)	< 1 μm, [nm size in (%)]	Misorientation angle (LAGB) (%)
400	2 passes	27.3	2.68	94.2
	10 Passes	17.6	4.41	86.3
300	2 passes	11.1	3.35	85.2
	6 passes	9.3	1.47	91.6
200	2 passes	6.4	2.65	78.6
	8 passes	3.3	9.34	58.7
Unprocessed alloy		84.5	0.02	60.3





**Fig. 9** TEM micrographs of CEE processed Al 5083 alloy specimens at 400 °C: **a** after 2 passes, **b** after 10 passes

#### 4 Discussion

Grain refinement is the net outcome of the positive effect of the imposed strain and the adverse effect of the test temperature. Therefore, the present results which emphasize the key role of temperature in determining the final grain size make good sense. The improvement in the strength properties at 400 °C and 300 °C is rather small. This is indicative of the dominance of dynamic recovery and re-crystallization processes over strain hardening [21]. Figure 2a also reveals that the strain distribution is non-uniform. At 300 °C, the

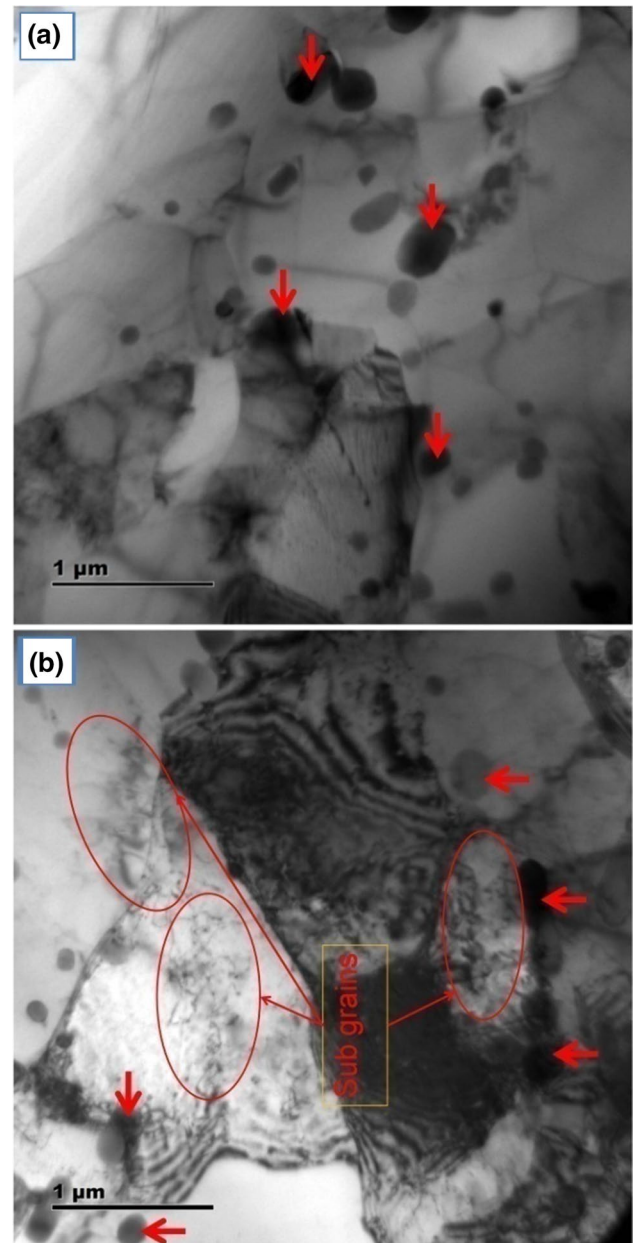


**Fig. 10** TEM micrographs of CEE processed Al 5083 alloy specimens at 300 °C: **a** after 2 passes, **b** after 6 passes

continuous reduction in hardness values is attributed to dynamic re-crystallization. A similar trend has been reported by other investigations also [42, 43]. Increase in grain size after 8 and 10 passes is traced to grain growth.

TEM micrograph of CEE processed Al 5083 alloy showed evidence for sub-grain formation (Figs. 10b, 11b). A few rod-like dispersoids/precipitates (red arrowed) were also seen. These second phase particles play a key role in grain refinement (by trapping dislocations [44]) and dislocation accumulation [44, 45] during the CEE process. Still, the UFG-/nano- grains volume was rather small and a significant

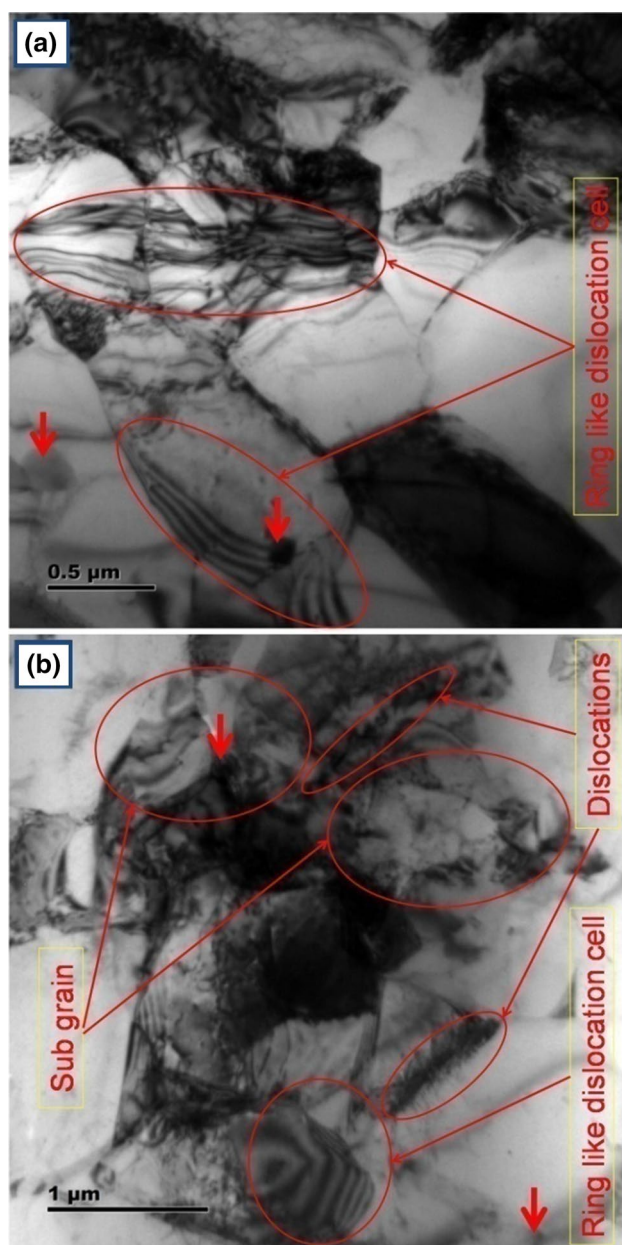


**Fig. 11** TEM micrographs of CEE processed Al 5083 alloy specimens at 200 °C: **a** after 2 passes, **b** after 8 passes

fraction of LAGBs was present due to the adverse effect of high temperatures, i.e. 400 °C and 300 °C, limited (medium level) strains imposed—see Figs. 9b and 10b after 10 passes at 400 °C and 6 passes at 300 °C respectively.

At 200 °C, due to the decreased temperature, strain hardening due to dislocation multiplication was dominant up-to the end of 6 passes (Fig. 2c) and there was a significant increase in hardness. After eight passes of CEE, dynamic re-crystallization and fresh grain formation/grain refinement was seen. The Mg element in solid solution and the Mg-precipitate particles formed along the boundaries hindered

dynamic re-crystallization by grain boundary/ precipitate (Orowan) pinning [10, 46]. The HAGB fraction had also increased to 42.3% (Fig. 8b). There is a suggestion that when both HAGBs and LAGBs are present in significant proportions, both dislocation strengthening and grain boundary strengthening are operative [17]. Therefore, the hardness value had increased after 8 passes of CEE. This is consistent with an earlier finding [15]. With increasing number of passes, homogeneity of deformation improved—see Fig. 2c.

TEM micrograph of CEE processed alloy after 8 passes at 200 °C reveals significant changes in the microstructure. No strain softening was seen and a high density of dislocations and sub-grains were present (Fig. 11b). Nature of strain hardening depends on the grain size distribution [47]. When the grains are ultrafine- or nano-grained, strain-rate-sensitivity could flow from the combined action of strain hardening and grain rotation [48]. In addition, the Mg-rich precipitates present in the alloy pin the grain boundaries and restrict grain rotation, which, in turn, could favor adiabatic shear band formation [49]. Some precipitates involving Cu, Fe and Mn could also be seen. After 8 CEE passes the microhardness was  $104 \pm 0.6$  HV. In contrast, a similar alloy, containing AlMg<sub>5</sub> precipitates, could reach a hardness value of 102HV only after 33 passes involving the CEC process [7].

At 200 °C after 10 passes due to re-crystallization and grain growth a decrease in strength properties is seen—Fig. 3c. Based on a comparison of microstructure and mechanical properties obtained at the three temperatures, it could be concluded that a lower processing temperature ensures homogeneous strain distribution, uniform grain refinement and consistent properties.

Similarly, Fig. 8b reveals that the average grain size after 8 passes of CEE at 200 °C ( $3.3 \pm 0.6$  μm) is 25 times finer than the parent (annealed) alloy ( $84.5 \pm 6.8$  μm). Evidently, DRX is the important reason contributing to this refinement of grains.

It is recognized that in duplex Al–Mg alloys, the Al phase is a soft phase compared with the α-Mg phase and the face centered cubic (FCC) structure of the Al phase possesses more slip systems compared with the hexagonal closed-packed (HCP) α-Mg phase [50]. Under severe strain, the Al phase is elongated steadily along the extrusion direction due to dislocations generation and the presence of α-Mg phase that modifies the deformation of the Al phase. Furthermore, due to high strains, the Al–Mg particles were fragmented and their fractions had become dispersive, and mostly distributed in the Al phase of the alloy. The microstructure formed consists of solid solution and dispersed precipitates [51].

The mechanical performance of the alloy after SPD was governed by two strengthening mechanisms: strain hardening and/or refinement of grains [52]. Strain/work hardening was a principal mechanism of metals and alloys that are

subjected to deformation processing. This mechanism is based on the principle of multiplication of dislocations, dislocation motion, and mutual interaction of dislocation [53]. During SPD process, the formation of random dislocations in grains leads to a significant rise in the yield strength and ultimate tensile strength values. In addition, the mechanical properties of metallic metals and alloys were also influenced by grain refinement. The reduction in grain size led to an increase in the number of grain boundaries acting as barriers to dislocation glide. On the other hand, the ductility of the materials decreases due to strain hardening, inhibition of dislocation movement and the fragmentation of sub-grain or dislocation cells [54].

Tsuji et al. [55] reported that the strain/work hardening effect in metals/alloys becomes difficult with a reduction in grain size. It is known that refinement of grains could improve the strength along with ductility simultaneously. The refinement of grains has an adverse influence on ductility. However, the influence of grain refinement is not so significant as that of strain hardening. Therefore, the elongation continues to decrease after 6 passes at 300 °C and 8 passes at 200 °C respectively. However, after 10 passes at 400 °C, the effects of grain refinement become more obvious, whereas the influence of strain hardening is reduced. Therefore, good ductility is noticed after the 10th pass than that of the previous passes (2–8 passes) of CEE at 400 °C.

The variations in micro-hardness values with respect to number of passes are presented in Fig. 2. It is evident that the hardness values increased with increase in the number of passes. In addition, a sudden rise was attained in the micro-hardness value (from  $51 \pm 1.9\text{HV}$  to  $65 \pm 1.2\text{HV}$  at 400 °C) after 2 passes, while great additional increases were noticed afterwards up-to 10 passes (micro-hardness value of  $82 \pm 1.2\text{HV}$  at 400 °C). The rapid increase at comparatively low strains could be correlated with strain hardening derived from dislocations and their interactions [56]. The error bars (variations of hardness) reveal that the strain is more homogeneous after processing at 200 °C. Also, it was clear that the strain homogeneity improved after higher number of passes in all the cases. Efficient grain reduction inhibits the free formation of dislocations due to which the enhancement in micro-hardness at higher number of passes is dominated by grain refinement mechanism (Hall–Petch effect) [57]. Higher CEE passes also help in the redistribution of the dislocations generated as uniform grain refinement is achieved. In all cases the hardness enhancement obeyed the Hall–Petch relation [58]. Similarly, it could be seen that after higher number of passes improved YS and UTS values as well as increased elongations could be seen at 400 °C and 300 °C (Fig. 3). Also, the increments in YS and UTS and the decrease in elongation are rather small, except in the case of the specimen processed at 200 °C. At higher passes, however, high strength and low elongation

resulted due to significant reduction in grain size. As the influence of strain hardening diminishes, steady evolution of UFG microstructure plays a dominant role in improving the strength and reducing the elongation [59].

The improved hardening behavior of UFG metals could be explained by considering the strengthening mechanisms. At elevated temperatures, even low strains led to an accumulation of high dislocation densities due to limited dynamic recovery. The present work reveals that the hardening behavior increases the dislocations mean free path after the 2nd pass of CEE. Further increases in strain increase the dislocations density, blocking of dislocation movements and formation of dislocation tangled zones. This phenomenon could be severe in UFG metals due to limited grain interior space and enhanced possibilities for the blockage of dislocations. A further increase in the number of CEE passes increases the accumulated strain leading to the formations of cell structure. Then further generation of dislocations becomes rather difficult. At this point, the microstructure consists of a cell structure with wide dislocation walls. A further increase in imposed strain converts the dislocation cells into UFG with HAGBs. Therefore, the increases in the micro-hardness values are high in the UFG metal. The maximum hardness value achieved after 8 passes at 200 °C in the UFG alloy was  $104 \pm 0.6\text{HV}$ .

Usually solid solution strengthening, dislocation strengthening and precipitation hardening influence the strength of metals and alloys in addition to grain reduction. According to Sheik et al. [60] the variations in YS and UTS values could be explained by the equation,

$$\frac{\sigma D}{Gb} = k \quad (1)$$

where,  $\sigma$ —is the tensile strength,  $D$ —is the sub-grain diameter,  $G$ —is the shear modulus,  $b$ —is the Burgers' vector of dislocations and  $k$ —is a dimensionless constant.

The tensile strength of a metal is directly proportional to the Burgers' vector of dislocations and the shear modulus (i.e., both are constants for a given metal) and inversely proportional to the sub-grain size. Grain refinement increases the tensile strength to a certain level, but beyond a possible number of passes the tensile strength reaches a plateau. The imposed strain, therefore, is connected to the temperature, which, in turn, influences the hardness value of the metal by accumulation of dislocations and grain refinement [8, 60].

The reasons for the variations in the micro-hardness values are mostly similar to those of the yield and tensile strength. The rapid increase in YS of the alloy was observed with refinement of grains as per Hall–Petch relation, see Fig. 4. The strengthening was also attended by strain hardening effect due to Mg- particles that retard the movement of dislocations. This leads to slopes of the Hall–Petch plots at 200 °C [61].



The present results are consistent with earlier findings [62, 63]. At 400 °C and 300 °C processing up-to 10 passes, higher ductility was exhibited for the fine grain sizes present, while a somewhat less ductility was associated with the UFG alloy at 200 °C. The specimens with UFG were harder and stronger compared with the coarser grain size (annealed) alloy. They were also strengthened to some extent by the Mg addition, which results in Al–Mg solid solution. Therefore, strain hardening and solid-solution strengthening are present. Additionally, the presence of Mg-particles in the Al matrix lowers the rate of recovery which leads to a higher strain hardening rate [15, 62, 64]. Homogeneous UFG structures were observed in the TEM images corresponding to the three different temperatures due to the increased number of grain boundaries, which, in turn, led to more dynamic sites for nucleation of new strain-free grains (dynamic recrystallization) (Fig. 7a–f). The differences in the hardness of the parent alloy (annealed) and the UFG material could be traced to the changes observed in the microstructure, grain size and misorientation angle distributions of the grain boundaries, as shown in Figs. 6, 7, 8 and Table 2.

The lower temperature processing improves the strength due to a higher fraction of HAGBs (after eight passes) and finer grain sizes (Eq. (1)). The decrease in ductility was due to sub-grain formation and the presence of thick dislocation cell/sub-grain walls [8, 65, 66].

The Hall–Petch relationship was obeyed at all the three processing temperatures. From the results it has become clear that the slope ( $k_y$ ) in the Hall–Petch equation is smaller and the intercept ( $\sigma_0$ ) larger for the specimens processed at 200 °C compared with those treated at 300 °C and 400 °C (Fig. 4).

## 5 Conclusions

The effects of cyclic expansion extrusion processing at different temperatures and number of passes on the mechanical properties and microstructures of Al–Mg alloy, AA 5083, were studied and the following conclusions could be drawn.

1. A decrease in CEE processing temperature and an increase in the degree of strain imparted resulted in an alloy of high dislocation density, fine grain size and a homogeneous microstructure. This gave rise to a monotonic increase in the strength properties. After processing at the high temperatures of 300 °C and 400 °C only insignificant grain refinement could be seen. The strength increase was marginal, but there was a noticeable increase in ductility.
2. At 200 °C, noticeable grain refinement, with a homogeneous microstructure, was achieved after 8 CEE passes. The UTS value had increased to  $189 \pm 2.1$  MPa and the

hardness value to  $104 \pm 0.6$  HV, which were respectively 64% and 104% higher than the corresponding values for the unprocessed alloy.

**Acknowledgements** The authors thank Prof. Indradev Samajdar, IIT Bombay, for extending the use of the EBSD facility. The authors also acknowledge the help of PSG College of Technology, Coimbatore, India for making available the HRTEM facility for this work.

## References

1. J.M. García-Infanta, A.P. Zhilyaev, A. Sharafutdinov, O.A. Ruano, F. Carreño, An evidence of high strain rate superplasticity at intermediate homologous temperatures in an Al–Zn–Mg–Cu alloy processed by high-pressure torsion. *J. Alloys Comp.* **473**, 163–166 (2009)
2. R.Z. Valiev, T.G. Langdon, Developments in the use of ECAP processing for grain refinement. *Rev. Adv. Mater. Sci.* **13**, 15–26 (2006)
3. R.Z. Valiev, R.K. Islamgaliev, I.V. Alexandrov, Bulk nanostructured materials from severe plastic deformation. *Prog. Mater. Sci.* **45**, 103–189 (2000)
4. A.P. Zhilyaev, T.G. Langdon, Using high-pressure torsion for metal processing: fundamentals and applications. *Prog. Mater. Sci.* **53**, 893–979 (2008)
5. Z. Horita, T. Fujinami, M. Nemoto, T.G. Langdon, Equal-channel angular pressing of commercial aluminum alloys: grain refinement, thermal stability and tensile properties. *Metall. Mater. Trans. A* **31**, 691–701 (2000)
6. S.H. Seyed Ebrahimi, K. Dehghani, J. Aghazadeh, M.B. Ghasemian, S. Zangeneh, Investigation on microstructure and mechanical properties of Al/Al–Zn–Mg–Cu laminated composite fabricated by accumulative roll bonding (ARB) process. *Mater. Sci. Eng. A* **718**, 311–320 (2018)
7. M. Richert, J. Richert, J. Zasadziński, S. Hawrylkiewicz, J. Długopolski, Effect of large deformations on the microstructure of aluminium alloys. *Mater. Chem. Phys.* **81**, 528–530 (2003)
8. N. Thangapandian, S. Balasivanandha Prabu, K.A. Padmanabhan, Effects of die profile on grain refinement in Al–Mg alloy processed by repetitive corrugation and straightening. *Mater. Sci. Eng. A* **649**, 229–238 (2016)
9. H. Lianxi, L. Yuping, W. Erde, Y. Yang, Ultrafine grained structure and mechanical properties of a LY12 Al alloy prepared by repetitive upsetting-extrusion. *Mater. Sci. Eng. A* **422**, 327–332 (2006)
10. M.R. Jandaghi, H. Pouraliakbar, M.K.G. Shiran, G. Khalaj, M. Shirazi, On the effect of non-isothermal annealing and multi-directional forging on the microstructural evolutions and correlated mechanical and electrical characteristics of hot-deformed Al–Mg alloy. *Mater. Sci. Eng. A* **657**, 431–440 (2016)
11. D.M. Fouad, A. Moataz, W.H. El-Garaihy, H.G. Salem, Numerical and experimental analysis of multi-channel spiral twist extrusion processing of AA5083. *Mater. Sci. Eng. A* **764**, 138216 (2019)
12. N. Pardis, B. Talebanpour, R. Ebrahimi, S. Zomorodian, Cyclic expansion-extrusion (CEE): A modified counterpart of cyclic extrusion-compression (CEC). *Mater. Sci. Eng. A* **528**, 7537–7540 (2011)
13. K.A. Padmanabhan, S. Balasivanandha Prabu, On the conflicts in the experimental results concerning the mechanical properties of ultra-fine grained and nanostructured materials: effects of processing routes and experimental conditions. *Mater. Sci. Forum* **683**, 3–54 (2011)

14. J.J. Rino, S. Balasivanandha Prabu, K.A. Padmanabhan, On the influence of repetitive corrugation and straightening on the microstructure and mechanical properties of AA 8090 Al–Li alloy. *Arch. Civ. Mech. Eng.* **18**, 280–290 (2018)
15. N. Thangapandian, S. Balasivanandha Prabu, K.A. Padmanabhan, Effect of temperature and velocity of pressing on grain refinement in AA5083 aluminum alloy during repetitive corrugation and straightening process. *Metall. Mater. Trans. A* **47**, 6374–6383 (2016)
16. J.J. Rino, I. Jayaram Krishnan, S. Balasivanandha Prabu, K.A. Padmanabhan, Influence of velocity of pressing in RCS processed AA8090 Al–Li alloy. *Mater. Charact.* **140**, 55–63 (2018)
17. N. Hansen, Hall–Petch relation and boundary strengthening. *Scr. Mater.* **51**, 801–806 (2004)
18. N.Q. Chinh, J. Gubicza, T. Czeppe, J. Lendvai, C. Xu, R.Z. Valiev, T.G. Langdon, Developing a strategy for the processing of age-hardenable alloys by ECAP at room temperature. *Mater. Sci. Eng. A* **516**, 248–252 (2009)
19. N. Fakhari, F. Fereshteh-Saniee, R. Mahmudi, Significant improvements in mechanical properties of AA5083 aluminum alloy using dual equal channel lateral extrusion. *Trans. Nonferrous Met. Soc. China* **26**, 3081–3090 (2016)
20. S. Najafi, A.R. Eivani, M. Samaee, H.R. Jafarian, J. Zhou, A comprehensive investigation of the strengthening effects of dislocations, texture and low and high angle grain boundaries in ultrafine grained AA6063 aluminum alloy. *Mater. Charact.* **136**, 60–68 (2018)
21. I. Mazurina, T. Sakai, H. Miura, O. Sitdikov, R. Kaibyshev, Effect of deformation temperature on microstructure evolution in aluminum alloy 2219 during hot ECAP. *Mater. Sci. Eng. A* **486**, 662–671 (2008)
22. A. Goloborodko, O. Sitdikov, R. Kaibyshev, H. Miura, T. Sakai, Effect of pressing temperature on fine-grained structure formation in 7475 aluminum alloy during ECAP. *Mater. Sci. Eng. A* **381**, 121–128 (2004)
23. V. Babu, S. Balasivanandha Prabu, K.A. Padmanabhan, Microstructure homogeneity in AA6063 alloy processed by cyclic expansion extrusion. *Defect Diffusion Forum* **385**, 223–227 (2018)
24. K.R. Cardoso, M.A. Munoz-Morris, K.V. León, D.G. Morris, Room and high temperature ECAP processing of Al–10% Si alloy. *Mater. Sci. Eng. A* **587**, 387–396 (2013)
25. S. Bathul, R.C. Anandani, A. Dhar, A.K. Srivastava, Microstructural features and mechanical properties of Al 5083/SiCp metal matrix nanocomposites produced by high energy ball milling and spark plasma sintering. *Mater. Sci. Eng. A* **545**, 97–102 (2012)
26. S.Y. Chang, B.D. Ahn, S.K. Hong, S. Kamado, Y. Kojima, D.H. Shin, Tensile deformation characteristics of a nano-structured 5083 Al alloy. *J. Alloys Compd.* **386**, 197–201 (2005)
27. B.B. Straumal, B. Baretzky, A.A. Mazilkin, F. Phillipp, O.A. Kogtenkova, M.N. Volkov, R.Z. Valiev, Formation of nanograined structure and decomposition of supersaturated solid solution during high pressure torsion of Al–Zn and Al–Mg alloys. *Acta Mater.* **52**, 4469–4478 (2004)
28. T.B. Massalski, et al. (eds.), *Binary Alloy Phase Diagrams* (ASM International, Materials Park, 1993), p. 3534
29. Y. Iwahashi, Z. Horita, M. Nemoto, T.G. Langdon, The process of grain refinement in equal-channel angular pressing. *Acta Mater.* **46**, 3317–3331 (1998)
30. T. Morishige, T. Hirata, T. Uesugi, Y. Takigawa, M. Tsujikawa, K. Higashi, Effect of Mg content on the minimum grain size of Al–Mg alloys obtained by friction stir processing. *Scr. Mater.* **64**, 355–358 (2011)
31. H. Huang, J. Zhang, Microstructure and mechanical properties of AZ31 magnesium alloy processed by multi-directional forging at different temperatures. *Mater. Sci. Eng. A* **674**, 52–58 (2016)
32. F. Liu, H. Yuan, J. Yin, J.T. Wang, Influence of stacking fault energy and temperature on microstructures and mechanical properties of fcc pure metals processed by equal-channel angular pressing. *Mater. Sci. Eng. A* **662**, 578–587 (2016)
33. P. Rodriguez-Calvillo, J.M. Cabrera, Microstructure and mechanical properties of a commercially pure Ti processed by warm equal channel angular pressing. *Mater. Sci. Eng. A* **625**, 311–320 (2015)
34. D. Singh, R. Jayaganthan, P. Nageswara Rao, A. Kumar, D. Venkateswarlu, Effect of initial grain size on microstructure and mechanical behavior of cryorolled AA 5083. *Mater. Today Proc.* **4**, 7609–7617 (2017)
35. G. Morris David, I. Gutierrez-Urrutia, M.A. Munoz-Morris, Analysis of strengthening mechanisms in a severely-plastically-deformed Al–Mg–Si alloy with submicron grain size. *J. Mater. Sci.* **42**, 1439–1443 (2007)
36. A. Chidambaram, S. Balasivanandha Prabu, K.A. Padmanabhan, Microstructure and mechanical properties of AA6061–5wt.% TiB<sub>2</sub> in-situ metal matrix composite subjected to equal channel angular pressing. *Mater. Sci. Eng. A* **759**, 762–769 (2019)
37. O. Sitdikov, E. Avtokratova, T. Sakai, K. Tsuzaki, Ultrafine-grain structure formation in an Al–Mg–Sc alloy during warm ECAP. *Metall. Mater. Trans. A* **44**, 1087–1100 (2013)
38. W. Guo, Q.D. Wang, B. Ye, M.P. Liu, T. Peng, X.T. Liu, H. Zhou, Enhanced microstructure homogeneity and mechanical properties of AZ31 magnesium alloy by repetitive upsetting. *Mater. Sci. Eng. A* **540**, 115–122 (2012)
39. A.L.D.M. Costa, A.C.D.C. Reis, L. Kestens, M.S. Andrade, Ultra grain refinement and hardening of IF-steel during accumulative roll-bonding. *Mater. Sci. Eng. A* **406**, 279–285 (2005)
40. K.T. Park, H.J. Kwon, W.J. Kim, Y.S. Kim, Microstructural characteristics and thermal stability of ultrafine grained 6061 Al alloy fabricated by accumulative roll bonding process. *Mater. Sci. Eng. A* **316**(1–2), 145–152 (2001)
41. F. Dalla Torre, R. Lapovok, J. Sandlin, P.F. Thomson, C.H.J. Davies, E.V. Pereloma, Microstructures and properties of copper processed by equal channel angular extrusion for 1–16 passes. *Acta Mater.* **52**, 4819–4832 (2004)
42. S.N. Alhajeri, N. Gao, T.G. Langdon, Hardness homogeneity on longitudinal and transverse sections of an aluminum alloy processed by ECAP. *Mater. Sci. Eng. A* **528**, 3833–3840 (2011)
43. V. Aferdita, M. Cabibbo, T.G. Langdon, A characterization of microstructure and microhardness on longitudinal planes of an Al–Mg–Si alloy processed by ECAP. *Mater. Charact.* **84**, 126–133 (2013)
44. S. Cheng, Y.H. Zhao, Y.T. Zhu, E. Ma, Optimizing the strength and ductility of fine structured 2024 Al alloy by nano-precipitation. *Acta Mater.* **55**, 5822–5832 (2007)
45. Y.H. Zhao, X.Z. Liao, S. Cheng, E. Ma, Y.T. Zhu, Simultaneously increasing the ductility and strength of nanostructured alloys. *Adv. Mater.* **18**, 2280 (2006)
46. S. Spriano, R. Doglione, Marcello Baricco, Texture, hardening and mechanical anisotropy in AA 8090-T851 plate. *Mater. Sci. Eng. A* **257**, 134–138 (1998)
47. H. Pirgazi, A. Akbarzadeh, R. Petrov, L. Kestens, Microstructure evolution and mechanical properties of AA1100 aluminum sheet processed by accumulative roll bonding. *Mater. Sci. Eng. A* **497**, 132–138 (2008)
48. Y.Z. Guo, Y.L. Li, Z. Pan, F.H. Zhou, Q. Wei, A numerical study of microstructure effect on adiabatic shear instability: application to nanostructured/ultrafine grained materials. *Mech. Mater.* **42**, 1020–1029 (2010)
49. A. Alam, D.D. Johnson, Structural properties and relative stability of (meta) stable ordered, partially ordered, and disordered Al–Li alloy phases. *Phys. Rev. B Condens. Matter Mater. Phys.* **85**, 144202 (2012)

50. R. Wu, Z. Qu, M. Zhang, Effects of the addition of Y in Mg–8Li–(1, 3) Al alloy. *Mater. Sci. Eng. A* **516**, 96–99 (2009)
51. T. Wang, H. Zheng, R. Wu, J. Yang, X. Ma, M. Zhang, Preparation of fine-grained and high-strength Mg–8Li–3Al–1Zn alloy by accumulative roll bonding. *Adv. Eng. Mater.* **18**, 304–311 (2016)
52. R. Jamaati, M.R. Toroghinejad, High-strength and highly-uniform composite produced by anodizing and accumulative roll bonding processes. *Mater. Des.* **31**, 4816–4822 (2010)
53. H.Y. Wu, G.Z. Zhou, Plastic anisotropy and strain-hardening behavior of Mg–6% Li–1% Zn alloy thin sheet at elevated temperatures. *J. Mater. Sci.* **44**, 6182–6186 (2009)
54. G. Nussbaum, P. Saintfort, G. Regazzoni, H. Gjestland, Strengthening mechanisms in the rapidly solidified AZ 91 magnesium alloy. *Scr. Mater.* **23**, 1079–1084 (1989)
55. N. Tsuji, Y. Ito, Y. Saito, Y. Minamino, Strength and ductility of ultrafine grained aluminum and iron produced by ARB and annealing. *Scr. Mater.* **47**, 893–899 (2002)
56. M. Shaarbaif, M.R. Toroghinejad, Nano-grained copper strip produced by accumulative roll bonding process. *Mater. Sci. Eng. A* **473**, 28–33 (2008)
57. N. Thangapandian, S. Balasivanandha Prabu, Effect of combined repetitive corrugation and straightening and rolling on the microstructure and mechanical properties of pure aluminum. *Metallogr. Microstruct. Anal.* **6**, 481–488 (2017)
58. D.H. Kang, T.W. Kim, Mechanical behavior and microstructural evolution of commercially pure titanium in enhanced multipass equal channel angular pressing and cold extrusion. *Mater. Des.* **31**, 54–60 (2010)
59. M.R. Rezaei, M.R. Toroghinejad, F. Ashrafizadeh, Effects of ARB and ageing processes on mechanical properties and microstructure of 6061 aluminum alloy. *J. Mater. Proc. Technol.* **211**, 1184–1190 (2011)
60. H. Sheikh, E. Paimozd, S.M. Hashemi, Work hardening of Duratherm 600 cobalt superalloy using repetitive corrugation and straightening process. *Russ. J. Non-Ferrous Met.* **51**, 59–61 (2010)
61. R. Armstrong, I. Godd, R.M. Douthwaite, N.J. Petch, The plastic deformation of polycrystalline aggregates. *Philos. Mag.* **7**, 45–58 (1962)
62. D. Singh, P.N. Rao, R. Jayaganthan, Effect of deformation temperature on mechanical properties of ultrafine grained Al–Mg alloys processed by rolling. *Mater. Des.* **50**, 646–655 (2013)
63. V.S. Sarma, K. Sivaprasad, D. Sturm, M. Heilmaier, Microstructure and mechanical properties of ultra fine grained Cu–Zn and Cu–Al alloys produced by cryorolling and annealing. *Mater. Sci. Eng. A* **489**, 253–258 (2008)
64. J. Gubicza, N.Q. Chinh, Z. Horita, T.G. Langdon, Effect of Mg addition on microstructure and mechanical properties of aluminum. *Mater. Sci. Eng. A* **387**, 55–59 (2004)
65. G. Faraji, M.M. Mashhadi, A.R. Bushroa, A. Babaei, TEM analysis and determination of dislocation densities in nanostructured copper tube produced via parallel tubular channel angular pressing process. *Mater. Sci. Eng. A* **563**, 193–198 (2013)
66. W.J. Kim, S.I. Hong, Y.H. Kim, Enhancement of the strain hardening ability in ultrafine grained Mg alloys with high strength. *Scr. Mater.* **67**, 689–692 (2012)

**Publisher's Note** Springer Nature remains neutral with regard to jurisdictional claims in published maps and institutional affiliations.